

Strongly modifiable decay and angle-dependent light intensity for an atom near active plasmonic structures: A macroscopic QED study

Ji-Yue Dai(戴吉月), Meng-Dan Zhao(赵梦丹), Yu Zhou(周昱), and Jun Xin(忻俊)
Citation: Chin. Phys. B, 2026, 35 (**2**): 027301. DOI: 10.1088/1674-1056/ae194d
http://cpb.iphy.ac.cn; http://iopscience.iop.org/cpb

What follows is a list of articles you may be interested in

Quantization of electromagnetic modes and angular momentum on plasmonic nanowires

Guodong Zhu(朱国栋), Yangzhe Guo(郭杨喆), Bin Dong(董斌), Yurui Fang(方蔚瑞)
Chin. Phys. B, 2020, 29 (8): 087301. DOI: 10.1088/1674-1056/ab9698

Research progress of femtosecond surface plasmon polariton

Yulong Wang(王玉龙), Bo Zhao(赵波), Changjun Min(闵长俊), Yuquan Zhang(张聿全), Jianjun Yang(杨建军), Chunlei Guo(郭春雷), Xiaocong Yuan(袁小聪)
Chin. Phys. B, 2020, 29 (2): 027302. DOI: 10.1088/1674-1056/ab6717

Room-temperature infrared photodetectors with hybrid structure based on two-dimensional materials

Tiande Liu(刘天德), Lei Tong(童磊), Xinyu Huang(黄鑫宇), Lei Ye(叶镭)
Chin. Phys. B, 2019, 28 (1): 017302. DOI: 10.1088/1674-1056/28/1/017302

Spoof surface plasmons resonance effect and tunable electric response of improved metamaterial in the terahertz regime

Wang Yue (王玥), Zhang Li-Ying (张丽颖), Mei Jin-Shuo (梅金硕), Zhang Wen-Chao (张文超), Tong Yi-Jing (童一静)
Chin. Phys. B, 2015, 24 (12): 127302. DOI: 10.1088/1674-1056/24/12/127302

Metallic nanowires for subwavelength waveguiding and nanophotonic devices

Pan Deng (潘登), Wei Hong (魏红), Xu Hong-Xing (徐红星)
Chin. Phys. B, 2013, 22 (9): 097305. DOI: 10.1088/1674-1056/22/9/097305

Strongly modifiable decay and angle-dependent light intensity for an atom near active plasmonic structures: A macroscopic QED study

Ji-Yue Dai(戴吉月), Meng-Dan Zhao(赵梦丹)[†], Yu Zhou(周昱)[‡], and Jun Xin(忻俊)

School of Science, Hangzhou Dianzi University, Hangzhou 310018, *China*

(Received 20 July 2025; revised manuscript received 28 October 2025; accepted manuscript online 30 October 2025)

Tunable plasmonic structures provide the possibility to actively modify the radiation from atoms through electromagnetic coupling. In this paper, we investigate the decay and radiation behavior of an atom near a dielectric nanosphere with conductive surface within the framework of macroscopic quantum electrodynamics. The electromagnetic fields including the losses in the materials can be taken as fundamental excitations which interact with the atom through a transition dipole. Both weak and strong coupling regimes have been investigated. The decay rate and the angle-dependent light intensities indeed strongly depend on the parameters of the system, i.e., the position and orientation of the dipole, the geometric size, and the surface conductivity, providing the opportunity of artificial control over these quantities. Generalizing the formalism in this paper to other systems, like metamaterials, is straightforward, which we believe may pave a way for future active quantum nanophotonic devices.

Keywords: plasmonics, quantum electrodynamics, light–matter interaction

PACS: 73.20.Mf, 32.50.+d

DOI: 10.1088/1674-1056/ae194d **CSTR:** 32038.14.CPB.ae194d

1. Introduction

Plasmonic nanostructures have the ability to confine light into ultra-small volumes with extremely large field intensities, which can lead to strong light–matter interactions and unprecedented sensitivities in optical detections.[1–5] Numerical approaches such as finite element method (FEM) and finite-difference time-domain (FDTD) method have been used to calculate the electromagnetic fields, where the materials are modeled by bulk permittivities.[6,7] As typical sizes of the nanostructures decrease, such description fails; quantum effects may occur.[8–12] The responses of electrons in metal are nonlocal in nature, and such nonlocality effect can be taken into account by the hydrodynamic model of electron fluids.[13–17] Shift of the resonant peaks in nanoparticles and dispersion relations have been discovered after including such nonlocality.[13,15] As the size goes atomic, time-dependent density functional theory is the better option. The fields can be calculated among the atoms giving a full quantum description of the electrons.[18–23] Hydrodynamic model can deal with the nonlocality, spill-out and even tunneling effects, and is much less computationally demanding but it can hardly take into account the details like charge transfer or atomic orbitals. More sophisticated model which considers surface responses has been proposed by introducing Feibelman parameters.[24] However, all the approaches mentioned above only consider the quantum aspect of matter. Further investigations of light–matter interaction in plasmonic nanostructures require also quantum description of the light.

Quantization of the electromagnetic fields in dispersive and lossy materials requires the introduction of some bosonic operators representing noise in the quantum system, which can take into account the material absorption.[25–31] Such operators are only phenomenological, but can preserve the widely known commutator held by the vector potential and electric fields.[25,26] The electric fields are linked to these operators through dyadic Green functions which are exactly the same as those in classic electrodynamics. The interaction between the fields and an atom is usually described by a traditional $-\boldsymbol{d}\cdot\boldsymbol{E}$ term; the whole Hamiltonian consists of three parts: the electromagnetic fields in dielectric, the atom and the one describing their interaction.[27,28] This formalism gives a satisfying quantum description of light–matter interactions in plasmonic nanostructures as well as in metamaterials. Traditional approaches also rely on the dyadic Green functions of the system and can give similar results;[32,33] however, the excitations of the photonic system are not incorporated into the framework of quantum theory. Recently, quasinormal mode approach has been proposed which is also fully compatible with the quantum theory.[34,35] These two methods not only resolve the limitations of classical theory but also offer parameter-free predictions of results in plasmonic and even chemical systems.[36,37]

In this paper, we take one little step further and investigate the radiation of a two-level atom near an active plasmonic nanostructure, i.e., a dielectric sphere with modifiable surface conductivity, within the framework of macroscopic QED. The

[†]Corresponding author. E-mail: Zmengdan_2017@163.com

[‡]Corresponding author. E-mail: yzhou@hdu.edu.cn

© 2026 Chinese Physical Society and IOP Publishing Ltd. All rights, including for text and data mining, AI training, and similar technologies, are reserved.

decay rate as well as angle-dependent intensity have been calculated based on the theory mentioned above. Rotating-wave approximation has been applied to simplify the light–atom interaction, and Markov approximation has been used to work out the time integrals, which is reasonable since our plasmonic nanostructure does not possess very strong resonances. The excited atom decays exponentially with a modified decay rate that is different to the one in vacuum. As for the light intensity, Markov approximation has also been applied and we get a relatively simple expression for the emitted intensity which is strongly tunable by changing the surface conductivity. Such formalism can be applied to investigate radiation of atoms near, for example, many kinds of metamaterials, providing an efficient way to derive the radiation feature of dipole sources within the quantum regime.

2. Methods

Figure 1 is the schematic illustration of the system, where an atom denoted by the red dot is placed on the z axis outside a sphere. The radius of the sphere is denoted as R, the permittivities of the materials outside and inside of the sphere are denoted as ε_1 and ε_2, respectively. The surface of the sphere is conductive (denoted by the dashed circle in Fig. 1), which throughout this paper is assumed to be graphene for simplicity. Thus, the surface conductivity can be tuned through external parameters, which is the Fermi level of graphene in this paper. In the calculations, spherical coordinates have been used, the dyadic Green functions are expanded using vector wave functions, and the decay rates as well as light intensities can be derived by summing over rather simple terms related to spherical Bessel or Hankel functions.

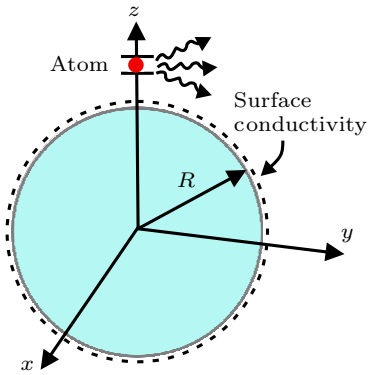


Fig. 1. Schematic of the system. A two-level atom is put near a dielectric nanosphere with a conductive surface. Red dot indicates the location of the two-level atom.

In macroscopic QED, the electric field with positive frequency can be expressed as

$$\hat{\boldsymbol{E}}^{+}(\boldsymbol{r},\omega)=\mathrm{i}\omega\mu_0\int \mathrm{d}^3\boldsymbol{r}'\overline{\overline{G}}_e(\boldsymbol{r},\boldsymbol{r}',\omega)\cdot\hat{\boldsymbol{j}}(\boldsymbol{r}',\omega), \tag{1}$$

where $\overline{\overline{G}}_e(\boldsymbol{r},\boldsymbol{r},'\omega)$ is the dyadic Green function, $\hat{\boldsymbol{j}}(\boldsymbol{r},\omega)=\omega\sqrt{\frac{\hbar\varepsilon_0}{\pi}\mathrm{Im}[\varepsilon(\boldsymbol{r},\omega)]}\hat{\boldsymbol{f}}(\boldsymbol{r},\omega)$ and $\hat{\boldsymbol{f}}(\boldsymbol{r},\omega)$ is the vector annihilation operator for the polaritonic excitation at position $\boldsymbol{r}$ and with frequency ω. $\hat{\boldsymbol{f}}(\boldsymbol{r},\omega)$ satisfies the bosonic commutation relation $[\hat{f}_i(\boldsymbol{r},\omega)\hat{f}_j(\boldsymbol{r}',\omega')]=\delta_{ij}\delta(\boldsymbol{r}-\boldsymbol{r}')\delta(\omega-\omega')$. The total Hamiltonian can be written as $\hat{H}=\hat{H}_{\mathrm{em}}+\hat{H}_{\mathrm{atom}}+\hat{H}_{\mathrm{int}}$, where $\hat{H}_{\mathrm{em}}=\int\mathrm{d}^3\boldsymbol{r}'\int_0^\infty\mathrm{d}\omega\hbar\omega\hat{\boldsymbol{f}}^{+}(\boldsymbol{r}',\omega)\cdot\hat{\boldsymbol{f}}(\boldsymbol{r}',\omega)$, $\hat{H}_{\mathrm{atom}}=\frac{1}{2}\hbar\omega_{\mathrm{A}}\hat{\sigma}_z$ and $\hat{H}_{\mathrm{int}}=-[\hat{\boldsymbol{\sigma}}^{+}\hat{\boldsymbol{E}}^{(+)}(\boldsymbol{r}_{\mathrm{atom}})\cdot\boldsymbol{d}+\mathrm{H.c.}]$. $\hat{\sigma}_z$, $\hat{\boldsymbol{\sigma}}^{+}$ and $\hat{\boldsymbol{\sigma}}^{-}$ are the usual Pauli matrices. ω_{A} is the transition frequency of the atom; $\boldsymbol{d}$ is the transition dipole, and H. c. stands for Hermitian conjugation. Rotating wave approximation has been applied, and the dispersions and losses of the materials have been taken into account in $\hat{H}_{\mathrm{em}}$. The wave function of the system can be expanded as

$$\begin{aligned}|\Psi(t)\rangle=&\,C_h(t)\,\mathrm{e}^{-\mathrm{i}\omega_{\mathrm{A}}t}|h\rangle|0\rangle+\int\mathrm{d}^3\boldsymbol{r}\int_0^\infty\mathrm{d}\omega C_{l,i}(\boldsymbol{r},\omega,t)\\&\times\mathrm{e}^{-\mathrm{i}\omega t}\mathrm{e}^{+\mathrm{i}\omega_{\mathrm{A}}t}|l\rangle|1_i(\boldsymbol{r},\omega)\rangle,\end{aligned} \tag{2}$$

where the $C_h(t)$ and $C_{li}(\boldsymbol{r},\omega,t)$ are slow-varying amplitudes. $|h\rangle|0\rangle$ denotes the state where the atom is excited and the rest of the system is vacuum; $|l\rangle|1_i(\boldsymbol{r},\omega)\rangle$ denotes the emitted atom with rest of the system in single-photon Fock state. After substituting Eqs. (1) and (2) into the Schrödinger equation and using the conditions $C_h(0)=1$ and $C_{li}(\boldsymbol{r},\omega,0)=0$, one can see that $C_h(t)$ and $C_{l,i}(\boldsymbol{r},\omega,t)$ obey the following equations:

$$\begin{aligned}\frac{\mathrm{d}C_h(t)}{\mathrm{d}t}=&-\frac{d_j}{\sqrt{\pi\hbar\varepsilon_0}}\int_0^\infty\mathrm{d}\omega\frac{\omega^2}{c^2}\int\mathrm{d}^3\boldsymbol{r}\sqrt{\mathrm{Im}[\varepsilon(\boldsymbol{r},\omega)]}\\&\times G_{ji}(\boldsymbol{r}_{\mathrm{a}},\boldsymbol{r},\omega)C_{l,i}(\boldsymbol{r},\omega,t)\,\mathrm{e}^{-\mathrm{i}(\omega-\omega_{\mathrm{A}})t},\end{aligned} \tag{3}$$

$$\begin{aligned}\frac{\mathrm{d}C_{l,i}(\boldsymbol{r},\omega,t)}{\mathrm{d}t}=&\frac{d_j}{\sqrt{\pi\hbar\varepsilon_0}}\frac{\omega^2}{c^2}\sqrt{\mathrm{Im}[\varepsilon(\boldsymbol{r},\omega)]}\\&\times G^{*}_{ji}(\boldsymbol{r}_{\mathrm{a}},\boldsymbol{r},\omega)C_h(t)\,\mathrm{e}^{\mathrm{i}(\omega-\omega_{\mathrm{A}})t},\end{aligned} \tag{4}$$

where $\boldsymbol{r}_{\mathrm{a}}$ and $\boldsymbol{r}$ denote respectively the positions of atom and photon. $\mathrm{Im}[\varepsilon(\boldsymbol{r},\omega)]$ is the imaginary part of the permittivity, and $i,j=\hat{r},\hat{\theta},\hat{\varphi}$ are indices denoting the directions. An integro differential equation of $C_h(t)$ can be obtained as

$$\frac{\mathrm{d}C_h(t)}{\mathrm{d}t}=\int_0^t\mathrm{d}t'K(t-t')C_h(t'),$$

where

$$\begin{aligned}K(t-t')=&-\frac{d_id_j}{\pi\hbar\varepsilon_0}\frac{\omega_{\mathrm{A}}^2}{c^2}\int_0^\infty\mathrm{d}\omega\,\mathrm{e}^{-\mathrm{i}(\omega-\omega_{\mathrm{A}})(t-t')}\\&\times\mathrm{Im}\,G_{ij}(\boldsymbol{r}_{\mathrm{a}},\boldsymbol{r}_{\mathrm{a}},\omega).\end{aligned} \tag{5}$$

By solving the above equation of $C_h(t)$, one gets

$$C_h(t)=1+\int_0^t\mathrm{d}t'K(t-t')C_h(t'), \tag{6}$$

where

$$\begin{aligned}K(t-t')=&\frac{d_id_j}{\pi\hbar\varepsilon_0}\frac{\omega_{\mathrm{A}}^2}{c^2}\int_0^\infty\mathrm{d}\omega[\mathrm{e}^{-\mathrm{i}(\omega-\omega_{\mathrm{A}})(t-t')}-1]\\&\times\frac{\mathrm{Im}\,G_{ij}(\boldsymbol{r}_{\mathrm{a}},\boldsymbol{r}_{\mathrm{a}},\omega)}{\mathrm{i}(\omega-\omega_{\mathrm{A}})}.\end{aligned}$$

According to the structure as shown in Fig. 1, only weak coupling may occur, thus Markov approximation applies, and

$$\frac{\mathrm{e}^{\mathrm{i}(\omega_{\mathrm{A}}-\omega)(t-t')}-1}{\mathrm{i}(\omega_{\mathrm{A}}-\omega)} \to \pi\delta(\omega_{\mathrm{A}}-\omega)+\mathrm{P}\frac{1}{\omega_{\mathrm{A}}-\omega},$$

where P means principal value. Finally, we have $\bar{K}(t-t') = -\frac{1}{2}\Gamma + \mathrm{i}\delta\omega$, where

$$\Gamma = \frac{2d_i d_j}{\hbar\varepsilon_0}\frac{\omega_{\mathrm{A}}^2}{c^2}\mathrm{Im}G_{ij}(\boldsymbol{r}_{\mathrm{a}},\boldsymbol{r}_{\mathrm{a}},\omega_{\mathrm{A}}). \tag{7}$$

The excited atom decays exponentially as $C_h(t) = \exp[(-\frac{1}{2}\Gamma+\mathrm{i}\delta\omega)t]$. Thus, the dyadic Green function contains all the information about how the atom decays near a plasmonic nanostructure. As for strong coupling regime, the dipole is coupled to one dominant resonance mode with very narrow line-width; thus, the imaginary part of the Green function can be assumed to be a peak with Lorentzian lineshape,[38] i.e.,

$$\mathrm{Im}G_{ij}(\boldsymbol{r}_{\mathrm{a}},\boldsymbol{r}_{\mathrm{a}},\omega) = \mathrm{Im}G_{ij}(\boldsymbol{r}_{\mathrm{a}},\boldsymbol{r}_{\mathrm{a}},\omega_{\mathrm{C}})\frac{\delta\omega_{\mathrm{C}}^2}{[\delta\omega_{\mathrm{C}}^2+(\omega-\omega_{\mathrm{C}})^2]}, \tag{8}$$

where ω_{C} and $\delta\omega_{\mathrm{C}}$ are the central angular frequency and width, respectively. Thus, $K(t-t')$ from Eq. (5) can be easily solved by extending the integral to $-\infty$ and the final expression is

$$\begin{aligned} K(t-t') &= -\frac{d_i d_j}{\hbar\varepsilon_0}\frac{\omega_{\mathrm{A}}^2}{c^2}\mathrm{Im}G_{ij}(\boldsymbol{r}_{\mathrm{a}},\boldsymbol{r}_{\mathrm{a}},\omega_{\mathrm{C}})\delta\omega_{\mathrm{C}} \\ &\quad\times \mathrm{e}^{-\mathrm{i}(\omega-\omega_{\mathrm{A}})(t-t')}\mathrm{e}^{-\delta\omega_{\mathrm{C}}(t-t')}. \end{aligned} \tag{9}$$

Thus, one can derive the differential equation for $C_h(t)$,

$$\ddot{C}_h(t)+[\mathrm{i}(\omega_{\mathrm{C}}-\omega_{\mathrm{A}})+\delta\omega_{\mathrm{C}}]\dot{C}_h(t)+\Omega^2 C_h(t)=0. \tag{10}$$

$\Omega^2 = \frac{d_i d_j}{\hbar\varepsilon_0}\frac{\omega_{\mathrm{A}}^2}{c^2}\mathrm{Im}G_{ij}(\boldsymbol{r}_{\mathrm{a}},\boldsymbol{r}_{\mathrm{a}},\omega_{\mathrm{C}})\delta\omega_{\mathrm{C}}$ and $\omega_{\mathrm{C}}\approx\omega_{\mathrm{A}}$. Since $\delta\omega_{\mathrm{C}}$ is very small and second-order terms can be neglected, it can be found that

$$C_h(t) = \exp\left(-\frac{\delta\omega_{\mathrm{C}}}{2}t\right)\cos(\Omega t), \tag{11}$$

which indicates damped Rabi oscillations. Now we give the details about finding the dyadic Green functions. Simple analytical solutions can only be found if the surface conductivity is isotropic. Here the surface conductivity has been taken from graphene for simplicity, which is a widely used two-dimensional material in plasmonics, showing huge potentials in applications. Since the materials are isotropic, the dyadic Green functions can be expressed by the usual vector wave functions in spherical coordinates. The vector wave functions needed here are

$$\begin{aligned} \boldsymbol{M}_{eo,mn} &= \mp\frac{m}{\sin\theta}Z_n(kr)P_n^m(\cos\theta)\begin{matrix}\sin(m\phi)\\ \cos(m\phi)\end{matrix}\hat{\theta} \\ &\quad -Z_n(kr)\frac{\mathrm{d}}{\mathrm{d}\theta}P_n^m(\cos\theta)\begin{matrix}\cos(m\phi)\\ \sin(m\phi)\end{matrix}\hat{\phi}, \\ \boldsymbol{N}_{eo,mn} &= \frac{n(n+1)}{kr}Z_n(kr)P_n^m(\cos\theta)\begin{matrix}\cos(m\phi)\\ \sin(m\phi)\end{matrix}\hat{r} \\ &\quad +\frac{1}{kr}\frac{\mathrm{d}}{\mathrm{d}r}[rZ_n(kr)]\left[\frac{\mathrm{d}}{\mathrm{d}\theta}P_n^m(\cos\theta)\begin{matrix}\cos(m\phi)\\ \sin(m\phi)\end{matrix}\hat{\theta}\right. \\ &\quad \left.\mp\frac{m}{\sin\theta}P_n^m(\cos\theta)\begin{matrix}\sin(m\phi)\\ \cos(m\phi)\end{matrix}\hat{\phi}\right], \end{aligned} \tag{12}$$

where k is the wavenumber in the medium, $Z_n(kr)$ is the Bessel function or Hankel function depending on the regions, $P_n^m(\cos\theta)$ is the associated Legendre polynomials. In the spherical coordinates, the transverse electric and transverse magnetic components of the fields are not coupled, and the dyadic Green function in every region differs from the one in vacuum representing the effects of transmission and reflection of waves. We have followed the standard procedure and got the expressions of the scattering dyadic Green functions for the regions inside (denoted as region 2) and outside (denoted as region 1) of the sphere,

$$\begin{aligned} &\overline{\overline{G}}_{es}^{21}(\boldsymbol{r},\boldsymbol{r}',\omega) \\ &= \frac{\mathrm{i}k_1}{4\pi}\sum_{\substack{mn\\ eo}}C_{mn}[D_M^{21}\boldsymbol{M}_{eo,mn}(k_2)\boldsymbol{M}_{eo,mn}^{(1)}(k_1) \\ &\quad +D_N^{21}\boldsymbol{N}_{eo,mn}(k_2)\boldsymbol{N}_{eo,mn}^{(1)}(k_1)], \end{aligned} \tag{14}$$

$$\begin{aligned} &\overline{\overline{G}}_{es}^{11}(\boldsymbol{r},\boldsymbol{r}',\omega) \\ &= \frac{\mathrm{i}k_1}{4\pi}\sum_{\substack{mn\\ eo}}C_{mn}[B_M^{11}\boldsymbol{M}_{eo,mn}^{(1)}(k_1)\boldsymbol{M}_{eo,mn}^{(1)}(k_1) \\ &\quad +B_N^{11}\boldsymbol{N}_{eo,mn}^{(1)}(k_1)\boldsymbol{N}_{eo,mn}^{(1)}(k_1)], \end{aligned} \tag{15}$$

where $C_{mn} = \frac{2n+1}{n(n+1)}\frac{(n-m)!}{(n+m)!}$, D_M^{21}, D_N^{21}, B_M^{11} and B_N^{11} are coefficients that depend on n. Since the atom is out of the sphere, the dyadic Green function in vacuum should take the form

$$\begin{aligned} \overline{\overline{G}}_0(\boldsymbol{r},\boldsymbol{r}',\omega) &= -\frac{\hat{r}\hat{r}}{k_1^2}\delta(r-r') \\ &\quad +\frac{\mathrm{i}k_1}{4\pi}\sum_{\substack{mn\\ eo}}C_{mn}[\boldsymbol{M}_{eo,mn}(k_1)\boldsymbol{M}_{eo,mn}^{(1)}(k_1) \\ &\quad +\boldsymbol{N}_{eo,mn}(k_1)\boldsymbol{N}_{eo,mn}^{(1)}(k_1)]. \end{aligned}$$

The surface of the sphere is conductive, thus the boundary conditions used are $\hat{r}\times(\overline{\overline{G}}_{es}^{11}+\overline{\overline{G}}_0) = \hat{r}\times\overline{\overline{G}}_{es}^{21}$, and $\hat{r}\times\nabla\times\overline{\overline{G}}_{es}^{21} - \hat{r}\times\nabla\times(\overline{\overline{G}}_{es}^{11}+\overline{\overline{G}}_0) = \mathrm{i}k_0 Z_0\sigma\hat{r}\times\hat{r}\times\overline{\overline{G}}_{es}^{21}$, where Z_0 is the vacuum impedance, σ is the surface conductivity and k_0 is the free space wavenumber. σ has been calculated from the model of graphene, which is

$$\begin{aligned} \sigma(\omega) &= \mathrm{i}\frac{e^2E_{\mathrm{F}}}{\pi\hbar^2}\frac{1}{\omega+\mathrm{i}\gamma}+\frac{e^2}{4\hbar}\left[\theta(\hbar\omega-2E_{\mathrm{F}})\right. \\ &\quad \left.+\frac{\mathrm{i}}{\pi}\ln\left|\frac{\hbar\omega-2E_{\mathrm{F}}}{\hbar\omega+2E_{\mathrm{F}}}\right|\right], \end{aligned}$$

where E_{F} is the Fermi level and $\gamma^{-1} = 0.35$ ps. We have applied the widely used conductivity model of graphene; using other models or even other materials may lead to similar conclusions. After substituting Eqs. (14) and (15) into these two boundary conditions, one finally derives the matrix equations determining the above mentioned four coefficients:

$$\begin{bmatrix} \frac{1}{R}\frac{\mathrm{d}}{\mathrm{d}r}\left[rj_n(k_2r)\right]_{r=R} - \mathrm{i}k_0Z_0\sigma j_n(k_2r) & -\frac{1}{R}\frac{\mathrm{d}}{\mathrm{d}r}\left[rh_n^{(1)}(k_1r)\right]_{r=R} \\ j_n(k_2R) & -h_n^{(1)}(k_1R) \end{bmatrix} \begin{bmatrix} D_M^{21} \\ B_M^{11} \end{bmatrix} = \begin{bmatrix} \frac{1}{R}\frac{\mathrm{d}}{\mathrm{d}r}[rj_n(k_1r)]_{r=R} \\ j_n(k_1R) \end{bmatrix}, \tag{16}$$

$$\begin{bmatrix} \frac{1}{Rk_2}\frac{\mathrm{d}}{\mathrm{d}r}\left[rj_n(k_2r)\right]_{r=R} & -\frac{1}{k_1R}\frac{\mathrm{d}}{\mathrm{d}r}\left[rh_n^{(1)}(k_1r)\right]_{r=R} \\ k_2j_n(k_2R) + \mathrm{i}k_0Z_0\sigma\frac{1}{Rk_2}\frac{\mathrm{d}}{\mathrm{d}r}\left[rj_n(k_2r)\right]_{r=R} & -k_1h_n^{(1)}(k_1R) \end{bmatrix} \begin{bmatrix} D_N^{21} \\ B_N^{11} \end{bmatrix} = \begin{bmatrix} \frac{1}{k_1R}\frac{\mathrm{d}}{\mathrm{d}r}[rj_n(k_1r)]_{r=R} \\ k_1j_n(k_1R) \end{bmatrix}, \tag{17}$$

where R is the radius of the sphere. Then, the complete dyadic Green functions in all spaces are known. From Eq. (7), it is clear that the decay rate at any position outside the sphere can now be calculated. By simply setting the conductivity to zero, one derives the usual boundary conditions that can be found in literature.

3. Results and discussion

Considering the symmetry of the structure, we focus on cases where the transition dipole of the atom is either parallel or perpendicular to the radial direction; the decay rates are denoted as Γ_{rr} and Γ_{tt}, respectively. Since the coupling between the dipole and the sphere is weak, Eq. (7) has been used. It will be convenient to compare these decay rates with the one in vacuum, i.e. normalized decay rates Γ_{rr}/Γ_0 and Γ_{tt}/Γ_0, where $\Gamma_0 = \frac{\omega_A^3 d^2}{3c^3\pi\hbar\varepsilon_0}$. $\overline{\overline{G}}^{11}_{es,rr}$ and $\overline{\overline{G}}^{11}_{es,tt}$ are the relevant quantities, which can be calculated by summing over infinite series as shown below. One can verify that the summation over the index m can be avoided given that the atom is located on the z axis, and only the terms with $m = 0$ contribute to the final result. Thus, one only needs to calculate the following equations:[31]

$$\overline{\overline{G}}^{11}_{es,rr} = \frac{\mathrm{i}k_1}{4\pi}\sum_{n=0}^{\infty}(2n+1)n(n+1)B_N^{11}\frac{\left[h_n^{(1)}(k_1r_\mathrm{a})\right]^2}{(k_1r_\mathrm{a})^2}, \tag{18}$$

$$\overline{\overline{G}}^{11}_{es,tt} = \frac{\mathrm{i}k_1}{8\pi}\sum_{n=0}^{\infty}(2n+1)\left\{B_M^{11}\left[h_n^{(1)}(k_1r_\mathrm{a})\right]^2 + B_N^{11}\left(\frac{1}{k_1r_\mathrm{a}}\right)^2\left[rh_n^{(1)}(k_1r_\mathrm{a})\right]'^2\right\}. \tag{19}$$

Two equations above involve summation over n. From spherical Hankel function of the first kind, one can know that summation over infinite series is not possible and convergence can be achieved by adding series with $n \le n_{\max}$. We have verified the convergence using $n_{\max} = 50$ within the frequency range in this paper. By substituting Eqs. (18) and (19) into Eq. (7), one can derive the normalized decay rates Γ_{rr}/Γ_0 and Γ_{tt}/Γ_0. Figure 2 shows these two quantities at three different locations, i.e., $r = 1.05R$, $1.1R$ and $1.15R$, where $R = 200$ nm, $E_\mathrm{F} = 0.1$ eV and the relative permittivity inside the sphere is 2.25. As the atom moves away from the sphere, Γ_{rr}/Γ_0 and Γ_{tt}/Γ_0 decrease rapidly. All curves exhibit oscillating behaviors which can be explained by wave interference. The onset energy of the interband transition of electrons in graphene is $2E_\mathrm{F}$. At low frequencies, the intraband transition part of the conductivity dominates, while the interband transition part of the conductivity plays a role at high frequencies. The radius of the sphere can also seriously affect the decay. Figure 3 shows the normalized decay rates in systems with three different sphere radii $R = 200$ nm, 250 nm, and 300 nm; other parameters are $r = 1.05R$, $E_\mathrm{F} = 0.1$ eV and the relative permittivity inside the sphere is again 2.25. Increasing R can obviously lower the decay rates meaning that small sphere has stronger light scattering effects in our system. We are more interested in tuning these decay rates via E_F. As shown in Fig. 4, increasing E_F may extend the frequency range where the decay rates show peaks. These peaks of the decay rates correspond to the effects of an optical cavity, i.e., Mie resonance modes denoted by n of the nanostructure, and increasing E_F can lead to variation of light–matter interactions in graphene which can explain the change in the separation between peaks in Fig. 4. The interband transition of electron in graphene mainly changes the decay rates when $E_\mathrm{F} = 0.1$ eV corresponding to the blue curves in Fig. 4, since this case has the lowest energy threshold. For lightly-doped graphene such as $E_\mathrm{F} = 0.1$ eV,

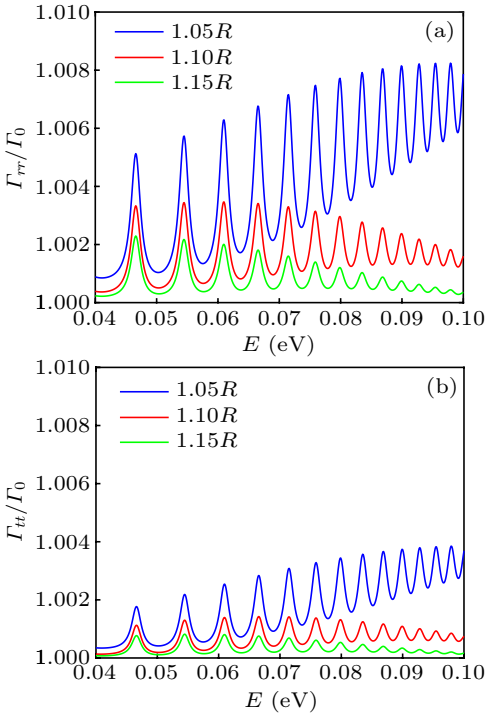


Fig. 2. (a) Normalized decay rates when the dipole is (a) perpendicular and (b) parallel to the spherical surface as functions of the photon energy. Blue, red and Green curves show the decay rates at three different distances from the surface, $r = 1.05R$, $1.1R$ and $1.15R$. Other parameters are $R = 200$ nm and $E_\mathrm{F} = 0.1$ eV.

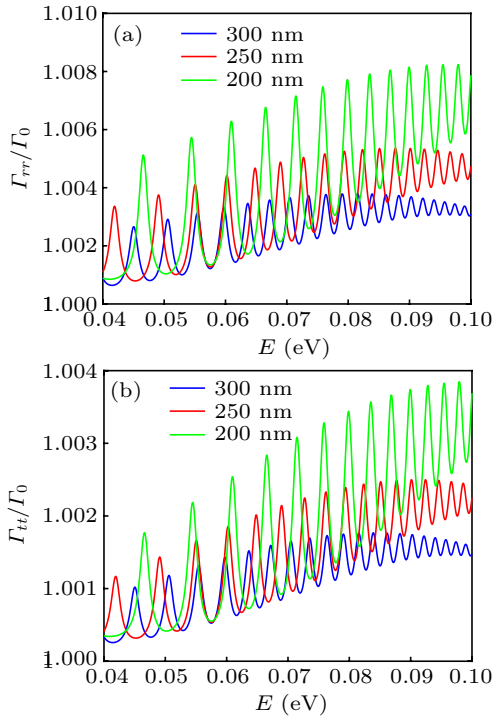


Fig. 3. Normalized decay rates when the dipole is (a) perpendicular and (b) parallel to the spherical surface as functions of the photon energy. Blue, red and Green curves show the decay rates at three different sphere radii, $R = 200$ nm, 250 nm, and 300 nm, respectively. Other parameters are $r = 1.05R$ and $E_{\rm F} = 0.1$ eV.

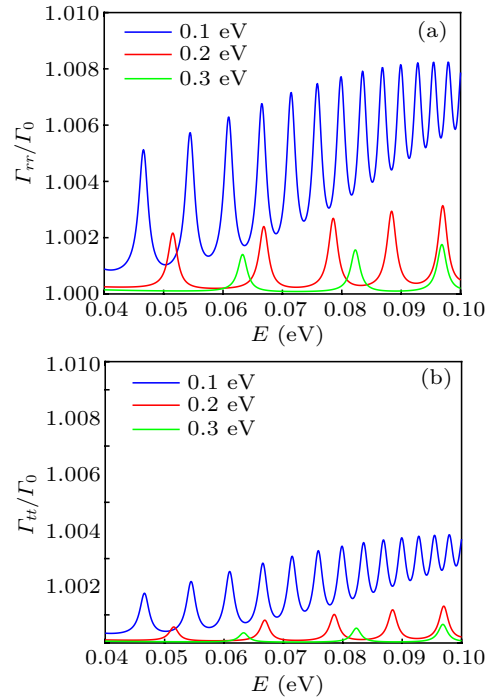


Fig. 4. Normalized decay rates when the dipole is (a) perpendicular and (b) parallel to the spherical surface at different electron doping levels. The ability to modify the decay rates through external parameters such as Fermi level is obvious. Other parameters are $R = 200$ nm and $r = 1.05R$.

the interband transition of electrons is important and cannot be neglected, while as one increases the Fermi energy the intraband part of the conductivity would dominate and then the interband transition can be neglected.

The light intensity radiated by the excited atom can be calculated as $I(\boldsymbol{r},t) = \langle\Psi(t)|\hat{E}^-(\boldsymbol{r})\cdot\hat{E}^+(\boldsymbol{r})|\Psi(t)\rangle$, where $\hat{E}^+(\boldsymbol{r}) = \int_0^\infty {\rm d}\omega\hat{E}^+(\boldsymbol{r},\omega)$ which can be easily derived from Eq. (1). By taking the Hermitian conjugate of $\hat{E}^+(\boldsymbol{r})$, one can get $\hat{E}^-(\boldsymbol{r})$. The time-dependent wavefunction is given by Eq. (2). After tedious but straightforward calculations, one finally gets the expression of the light intensity, which is

$$I(\boldsymbol{r},t) = \sum_i \left|\frac{\omega_{\rm A}^2 d_j}{\pi\varepsilon_0 c^2}\int_0^\infty {\rm d}\omega\,{\rm Im}\,G_{ji}(\boldsymbol{r}_{\rm a},\boldsymbol{r},\omega) \times\int_0^t {\rm d}t' C_h(t')\,{\rm e}^{-{\rm i}(\omega-\omega_{\rm A})(t-t')}\right|^2, \tag{20}$$

where i and j are indices denoting the directions. Markov approximation can be applied to drastically simplify the calculations. By replacing $C_h(t')$ with $C_h(t)$, i.e., moving $C_h(t')$ out of the integral, and approximating the time integral as we did in deriving Eq. (7), the expression of the intensity can be written as

$$I(\boldsymbol{r},t) = \sum_i \left|\frac{\omega_{\rm A}^2 d_j}{\varepsilon_0 c^2}\,{\rm Im}\,G_{ji}(\boldsymbol{r}_{\rm a},\boldsymbol{r},\omega_{\rm A})\right|^2 {\rm e}^{-\Gamma t}, \tag{21}$$

where the exponential decay comes from $C_h(t)$. Now we focus on the cases where the transition dipole is along the radial direction, and demonstrate the fact that the light intensity can be seriously modified. It would be more convenient to calculate the normalized intensity defined as $I(\boldsymbol{r},t)/I_0(\boldsymbol{r},t)$ omitting ${\rm e}^{-\Gamma t}$ and $I_0(\boldsymbol{r},t)$ is the intensity in vacuum. Considering the symmetry of the system and the fact that $j = \hat{r}$, only summation over the contributions from ${\rm Im}\,G_{rr}$ and ${\rm Im}\,G_{r\theta}$ is required. Again, only the terms with $m = 0$ need to be considered. If $r_{\rm a} > r$, contribution from ${\rm Im}\,G_{rr}$ can be written as

$${\rm Im}\left\{{\rm i}\sum_n \frac{2n+1}{k_1 r_{\rm a}} h_n^{(1)}(k_1 r_{\rm a})\,\frac{n(n+1)}{k_1 r} \times[j_n(k_1 r) + B_N^{11} h_n^{(1)}(k_1 r)]P_n(\cos\theta)\right\}, \tag{22}$$

and from ${\rm Im}\,G_{r\theta}$, it is

$${\rm Im}\left\{{\rm i}\sum_n \frac{2n+1}{k_1 r_{\rm a}} h_n^{(1)}(k_1 r_{\rm a})\left[\frac{[r j_n(k_1 r)]'}{k_1 r} + B_N^{11}\frac{[r h_n^{(1)}(k_1 r)]'}{k_1 r}\right]P_n'(\cos\theta)(-\sin\theta)\right\}. \tag{23}$$

If $r_{\rm a} < r$, contribution from ${\rm Im}\,G_{rr}$ can be written as

$${\rm Im}\left\{{\rm i}\sum_n \frac{2n+1}{k_1 r_{\rm a}}[j_n(k_1 r_{\rm a}) + B_N^{11} h_n^{(1)}(k_1 r_{\rm a})] \times\frac{n(n+1)}{k_1 r} h_n^{(1)}(k_1 r)\,P_n(\cos\theta)\right\}, \tag{24}$$

and from ${\rm Im}\,G_{r\theta}$, it is

$${\rm Im}\left\{{\rm i}\sum_n \frac{2n+1}{k_1 r_{\rm a}}[j_n(k_1 r_{\rm a}) + B_N^{11} h_n^{(1)}(k_1 r_{\rm a})] \times\frac{[r h_n^{(1)}(k_1 r)]'}{k_1 r}\right]P_n'(\cos\theta)(-\sin\theta)\right\}. \tag{25}$$

The expressions for vacuum can be found by setting $B_N^{11} = 0$. We have plotted the normalized total intensities under different levels of doping in Figs. 5 and 6, and their principal parts have been omitted as usual.[31] Figure 5 shows the angle-dependent intensities when $r < r_a$, other related parameters are $R = 200$ nm, $E = 0.3$ eV, $r = 240$ nm, $r_a = 260$ nm; figure 6 shows angle-dependent intensities when $r > r_a$, other related parameters are $R = 200$ nm, $E = 0.3$ eV, $r = 240$ nm and $r_a = 220$ nm. Increasing E_F can lead to stronger light–matter interactions which explains the fact that the light intensity from the atom becomes larger and more concentrated in some direction. Please note that distributions in Figs. 5 and 6 are near-field; in the space away from the system, the intensity distribution is similar to that of a dipole. Such field concentration is not related to the Kerker effect which usually requires careful design of the geometric parameters. As for strong coupling regime, the intensity exhibits Rabi oscillations. The Markov approximation cannot be used and one should carry out the integral using Eq. (11). After tedious calculations, one gets the expression for the intensity as

$$I(\boldsymbol{r},t) = \sum_i \left| \frac{\omega_A^2 d_j}{\varepsilon_0 c^2} \operatorname{Im} G_{ji}(\boldsymbol{r}_a, \boldsymbol{r}, \omega_C) \frac{\delta\omega_C}{\Omega} \right|^2 \times \mathrm{e}^{-\delta\omega_C t} \sin^2(\Omega t). \tag{26}$$

As for optical systems existing dominant resonance mode with very narrow line-width, it is more likely that one should apply the equations in the strong coupling regime where Rabi oscillation is the main feature.

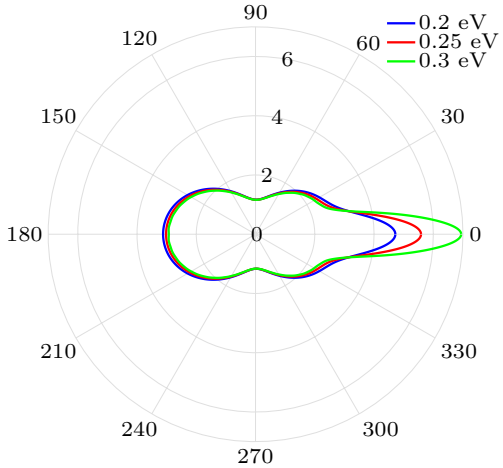


Fig. 5. Angle-dependent normalized light intensity at three different doping levels, where $r < r_a$. Other parameters are $R = 200$ nm, photon energy $E = 0.3$ eV, $r = 240$ nm, $r_a = 260$ nm.

Extending these calculations to the case where a dipole is placed near, for example, a spheroid is straightforward, and the dyadic Green functions can be constructed using special orthogonal vectorial functions; however, calculation of quantities such as decay rate and light intensity is not easy since the angular parts in the functions are no longer usual Legendre polynomials and one cannot derive simple expressions. In other systems like nanocubes, sophisticated numerical software packages may be used to calculated the dyadic Green functions. Extending the formalism to systems with many atoms is straightforward; however, one may not derive concise expressions for the decay rate or intensity, and usually needs to solve coupled differential equations directly. Based on these considerations, this formalism is more suitable for the system where a few atoms are coupled to nanostructures of which the dyadic Green functions can be acquired with high accuracy.

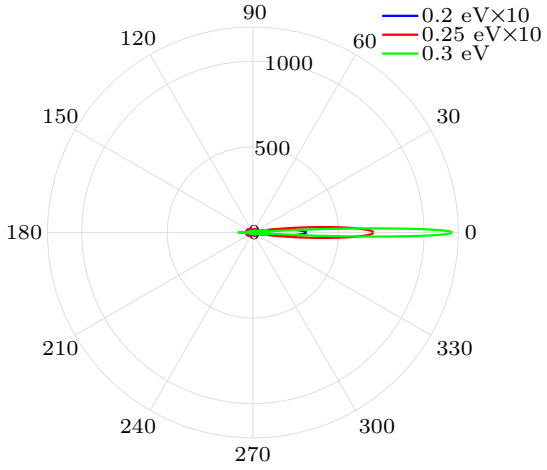


Fig. 6. Angle-dependent normalized light intensity at three different doping levels, where $r > r_a$. The blue and red curves have been magnified by 10 times for clarity. Other parameters are $R = 200$ nm, photon energy $E = 0.3$ eV, $r = 240$ nm and $r_a = 220$ nm.

4. Conclusions

In this paper, we have investigated the decay of an excited two-level atom near an active plasmonic nanostructure which is a dielectric sphere with a conductive surface. The dyadic Green functions inside and outside the sphere have been derived by matching the boundary conditions. The decay rates parallel and perpendicular to the radial directions have been derived both in the weak and strong coupling regimes, and can be strongly modified by changing the orientation of the transition dipole, the geometric parameters, and the surface conductivity. In the end, the electric fields radiated from the atom have been calculated whose angular distributions can also be actively tuned. The formalism used in this paper can be applied to investigate the radiation of an excited atom near other complex nanostructures, providing a new way to design nanophotonic devices within the quantum regime.

Acknowledgements

M. D. Zhao was supported by Hangzhou Dianzi University (Grant No. KYS075621018). J. Xin was supported by the Natural Science Foundation of Zhejiang Province (Grant No. LY24A050004).

References

[1] Maier Stefan A 2006 *Opt. Express* **14** 1957

[2] Kim S, Jin J, Kim Y J, Park I Y, Kim Y and Kim S W 2008 *Nature* **453** 757

[3] Ciracì C, Hill R T, Mock J J, Urzhumov Y, Fernández-Domínguez A I, Maier S A, Pendry J B, Chilkoti A and Smith D R 2012 *Science* **337** 1072

[4] Marinica D C, Kazansky A K, Nordlander P, Aizpurua J and Borisov A G 2012 *Nano Lett.* **12** 1333

[5] Thongrattanasiri S and García de Abajo F J 2013 *Phys. Rev. Lett.* **110** 187401

[6] Degiron A and Smith D R 2006 *Opt. Express* **14** 1611

[7] Amirjani A and Sadrnezhaad S K 2021 *J. Mater. Chem. C* **9** 9791

[8] Esteban R, Borisov A G, Nordlander P and Aizpurua J 2012 *Nat. Commun.* **3** 825

[9] Tame M S, McEnery K R, Özdemir Ş K, Lee J, Maier S A and Kim M S 2013 *Nat. Phys.* **9** 329

[10] Teperik T V, Nordlander P, Aizpurua J and Borisov A G 2013 *Opt. Express* **21** 27306

[11] Kulkarni V, Prodan E and Nordlander P 2013 *Nano Lett.* **13** 5873

[12] Zhu W, Esteban R, Borisov A G, Baumberg J J, Nordlander P, Lezec H J, Aizpurua J and Crozier K B 2016 *Nat. Commun.* **7** 11495

[13] García de Abajo F J 2008 *J. Phys. Chem. C* **112** 17983

[14] Fernández-Domínguez A I, Wiener A, García-Vidal F J, Maier S A and Pendry J B 2012 *Phys. Rev. Lett.* **108** 106802

[15] Mortensen N A, Raza S, Wubs M, Søndergaard T and Bozhevolnyi S I 2014 *Nat. Commun.* **5** 3809

[16] Tserkezis C, Stefanou N, Wubs M and Mortensen N A 2016 *Nanoscale* **8** 17532

[17] Lundeberg M B, Gao Y, Asgari R, Tan C, Duppen B V, Autore M, Alonso-González P, Woessner A, Watanabe K, Taniguchi T, Hillenbrand R, Hone J, Polini M and Koppens F H L 2017 *Science* **357** 187

[18] Chen H, McMahon J M, Ratner M A and Schatz G C 2010 *J. Phys. Chem. C* **114** 14384

[19] Marinica D C, Zapata M, Nordlander P, Kazansky A K, Echenique P M, Aizpurua J and Borisov A G 2015 *Sci. Adv.* **1** 1501095

[20] Varas A, García-González P, Feist J, García-Vidal F J and Rubio A 2016 *Nanophotonics* **5** 409

[21] Asadi-Aghbolaghi M, Rüger R, Jamshidi Z and Visscher L 2020 *J. Phys. Chem. C* **124** 7946

[22] Herring C J and Montemore M M 2023 *ACS Nanosci. Au* **3** 269

[23] Bonafé F P, Albar E I, Ohlmann S T, Kosheleva V P, Bustamante C M, Troisi F, Rubio A and Appel H 2025 *Phys. Rev. B* **111** 085114

[24] Yang Y, Zhu D, Yan W, Agarwal A, Zheng M, Joannopoulos J D, Lalanne P, Christensen T, Berggren K K and Soljačić M 2019 *Nature* **576** 248

[25] Matloob R, Loudon R, Barnett S M and Jeffers J 1995 *Phys. Rev. A* **52** 4823

[26] Matloob R and Loudon R 1996 *Phys. Rev. A* **53** 4567

[27] Gruner T and Welsch D G 1996 *Phys. Rev. A* **53** 1818

[28] Dung H T, Knöll L and Welsch D G 1998 *Phys. Rev. A* **57** 3931

[29] Matloob R 1999 *Phys. Rev. A* **60** 50

[30] Shahbazyan T V 2016 *Phys. Rev. Lett.* **117** 207401

[31] Behbahani M M, Amooghorban E and Mahdifar A 2016 *Phys. Rev. A* **94** 013854

[32] Gu Y, Wang L, Ren P, Zhang J, Zhang T, J F Martin O and Gong Q H 2012 *Nano Lett.* **12** 2488

[33] K Jha P, Ni X, Wu C, Wang Y and Zhang X 2015 *Phys. Rev. Lett.* **115** 025501

[34] Yan W, Faggiani R and Lalanne P 2018 *Phys. Rev. B* **97** 205422

[35] Zhou Q, Lin S P, Zhang P and Chen X W 2019 *Acta Phys. Sin.* **68** 147104 (in Chinese)

[36] Rivera N and Kaminer I 2020 *Nat. Rev. Phys.* **2** 538

[37] Hsu L Y 2025 *J. Phys. Chem. Lett.* **16** 1604

[38] Dung H T, Knöll L and Welsch D G 2000 *Phys. Rev. A* **62** 053804